Simulation Study of Elastic Micropropulsion Mechanism Modeled on Bending Mechanism of Eukaryotic Flagella in Liquid*

Shunichi KOBAYASHI**, Osamu TAKIZAWA***
and Hirohisa MORIKAWA**

The application of the dynamics in organisms to the field of engineering is very instructive. We noted the utility of eukaryotic flagellar motion for the propulsion of micromachines in liquid, and proposed a micropropulsion mechanism modeled on the active sliding of microtubules in eukaryotic flagella. The bending movement and the thrust force of the mechanism were simulated. For the modeling in the simulation, we took account of the elasticity of the micropropulsion mechanism. The influences of elasticity, maximum sliding length and viscosity of liquid on the bending movement and the thrust force were discussed.

Key Words: Flagella, Flagellar Motion, Propulsion, Micromachine, Biomechanics, Robotics

1. Introduction

Since most organisms are fairly autonomic, functional and efficient, the study of machines modeled on the motions of organisms is very significant in the engineering field. From this point of view, we aimed at examining the micropropulsion mechanism modeled on microorganisms in water. The active sliding of microtubules in flagella of eukaryotic organisms such as spermatozoa generates flagellar motion. Sugino and Naitoh[1),(2)] carried out a computer simulation of ciliary movements based on the distribution of actively sliding regions of microtubules. Since the cilia and the flagella share a common basic mechanism, this simulation is also appropriate for examining flagellar motion. We noted that the mechanism of the active sliding of microtubules would provide a good model for an artificial micropropulsion mechanism, and proposed a micropropulsion mechanism in liquid modeled on the bending mechanism of eukaryotic flagella. First, we simulated bending movement and thrust force characteristics of a two-dimensional micropropulsion mechanism using two microtubules and a three-dimensional micropropulsion mechanism using three microtubules[3),(4)]. The movements of both micropropulsion mechanisms were similar to flagellar motion; however, the simulation models were simplified by neglecting the elasticity of the micropropulsion mechanism. Hence, we improved on the simulation model by adding the elasticity of the micropropulsion mechanism and termed it the "elastic flagellar model". In this study, we examine the influence of elasticity on bending movement, and evaluate the relationship between thrust force and elasticity. Furthermore, we change the viscosity of liquid and discuss bending movement and thrust force characteristics.

* Received 14th June, 2000

** Department of Functional Machinery and Mechanics, Faculty of Textile Science and Technology, Shinshu University, 3-15-1 Tokida, Ueda, Nagano 386-8567, Japan. E-mail: shukoba@giptc.shinshu-u.ac.jp

*** Graduate School of Science and Technology, Shinshu University, 3-15-1 Tokida, Ueda, Nagano 386-8567, Japan

2. Nomenclature

A: amplitude
a: distance between adjacent microtubules
C_T: tangential component of viscous drag

coefficient
C_N : normal component of viscous drag coefficient
D : diameter of the elastic flagellar model
ds : microlength segment
E : Young's modulus of the elastic flagellar model
e_s : extent of sliding region
$e_{s\max}$: maximum extent of sliding region
F_x : x-directional thrust force
$\bar{F}_x$: average of x-directional thrust force
f : bending frequency
f_{eN} : normal component of the force acting on the microlength
f_{vN} : normal component of the viscous drag force on microlength
f_{vT} : tangential component of viscous drag force on microlength
f_x : Thrust force on the microlength
I : geometrical moment of inertia of the elastic flagellar model
l_s : sliding length
$l_{s\max}$: maximum sliding length
M_a : active bending moment exerted by sliding of microtubules
M_e : moment produced by an elastic back force under the influence of viscosity
M_v : moment produced by a viscous resistance
r_c : radius of bending curve
S_{TL} : total length of the elastic flagellar model
s : distance between the original coordinate axes and an arbitrary point along the longitudinal axis
s_{sl} : distance between the origin of the coordinate axes and the end of the sliding region along the longitudinal axis
t : time
t_{end} : ending time for calculation
v : propagation speed of each region
v_x, v_y : x and y directional moving velocities of microlength segment
ΔL_{DP} : longitudinal difference in the distribution pattern between two pairs of microtubules
ΔF_x : difference of the x-directional thrust force ($=F_{x\max}-F_{x\min}$)
Δt : a small fraction of time
θ : bending angle of a pair of microtubules
λ : wavelength
μ : coefficient of viscosity
ϕ : angle at which tangential line of ds intersects the x axis

3. Bending Mechanism of Flagella[5],[6]

Figure 1 shows a typical structure of a flagellum of sea urchin spermatozoa. The diameter of a single flagellum is about 0.2 μm. Nine outer doublet microtubules and a central pair of singlet microtubules are arranged in the cross section in this figure. Dyneins are located along the microtubule at intervals of 24 nm. A dynein has the force (1 - 4 pN) to move an adjacent microtubule toward the tip of a flagellum. We call this active sliding part of dyneins the "sliding region". Regions that resist active sliding and passive bending exist in the flagella, and we call these the "fixing region" and "bending region", respectively. When active sliding occurs, microtubules are bent by the configuration of the three regions shown in Fig. 2. Propagable waves are generated by moving each region toward the tip of a flagellum. The bending of flagellum occurs in a plane, which is shown in Fig. 1. If dyneins on the right half (doublets 1-5) of the cross section of the axoneme, especially dyneins on doublet 3, are active, active sliding occurs between doublets 3 and 4 and at the same time, 'passive' sliding occurs between doublets 7 and 8. The bending of flagellum

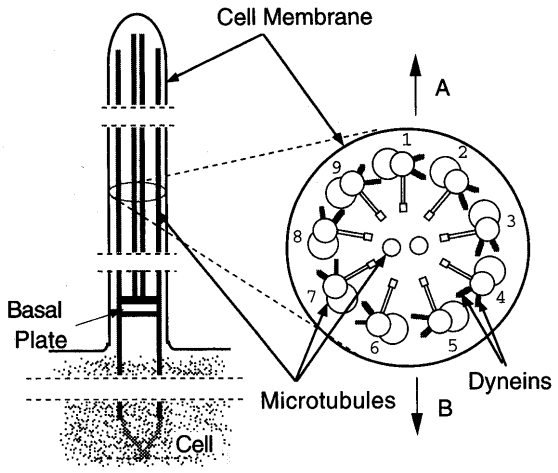

Fig. 1 Typical structure of a single flagellum. Arrows indicate the direction of planar bending.

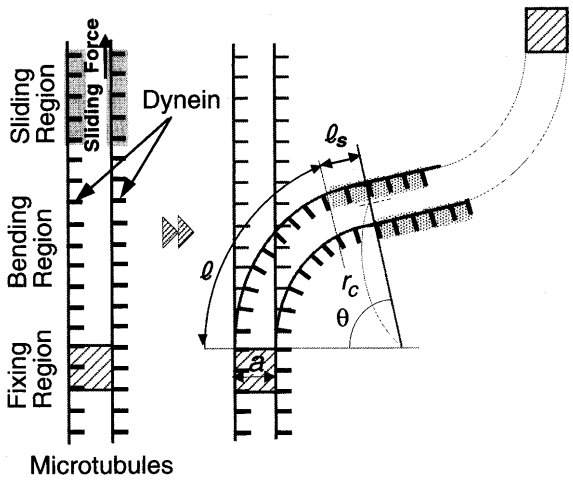

Fig. 2 Bending mechanism

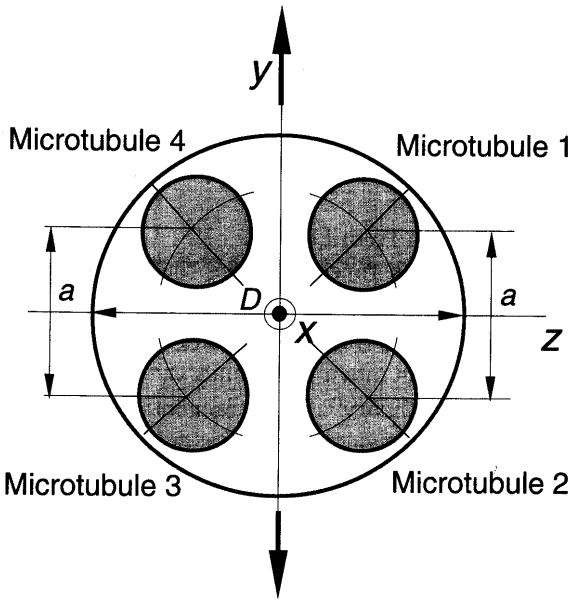

Fig. 3 Arrangement of microtubules

occurs in the direction shown by arrow B. If dyneins on the left half (doublets 6 - 9) of the cross section of the axoneme, especially dyneins on doublet 7, are active, the sliding direction is reversed and flagellum bents toward the opposite side (arrow A).

4. Basic Conditions for Modeling

The basic conditions for constructing the elastic flagellar model were as follows.

(1) Bending radius and bending angle in Fig. 2 can be formulated as

$$r_c=a\left(\frac{1}{2}+\frac{l}{l_s}\right), \tag{1}$$

$$\theta=\frac{l_s}{a}. \tag{2}$$

(2) The model consists of four outer microtubules without a central pair of microtubules. Figure 3 shows the arrangement of microtubules. This is the simplified model of the two subsets of sliding in flagellum.

(3) Active sliding occurs between the two pairs of microtubules 1 and 2, and microtubules 3 and 4, as shown in Fig. 4. There is no sliding between microtubules 2 and 3, and microtubules 4 and 1. Microtubules 1 and 3 drive microtubules 2 and 4 toward the end of the elastic flagellar model (corresponding to the tip of flagellum), respectively, when active sliding occurs.

(4) The basal cell such as a sperm head is ignored in the modeling.

(5) The center of the cross section on the top (corresponding to the basal position of flagellum) of the elastic flagellar model is located at the origin of the coordinate axes.

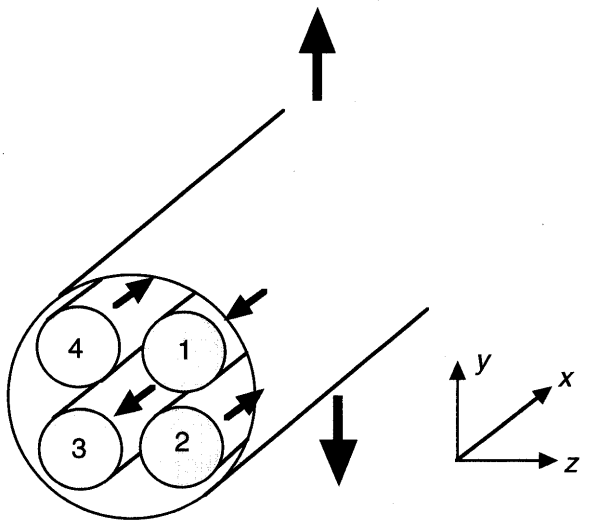

Fig. 4 Directions of active sliding

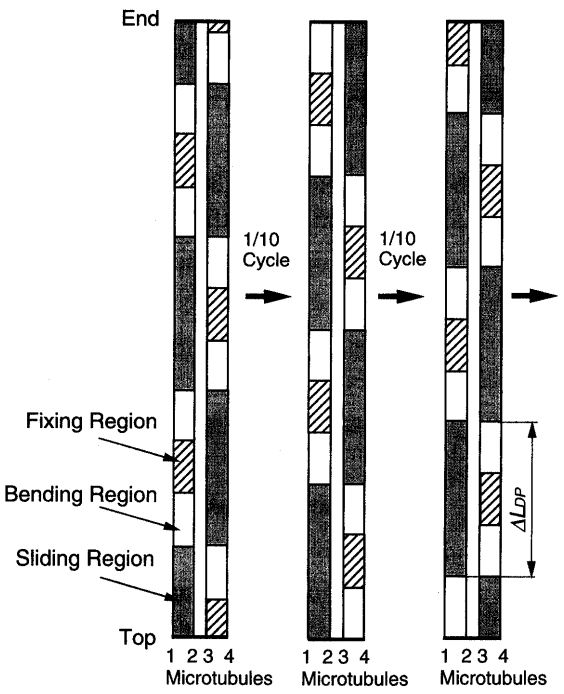

Fig. 5 Distribution pattern of each region

(6) The maximum number of sliding regions in each pair of microtubules is three.

Figure 5 shows the distribution pattern of each region. Each region propagates at a speed of v, which is given by

$$v=fS_{TL}, \tag{3}$$

where f is bending frequency and S_{TL} is total length of the elastic flagellar model. The longitudinal difference in the distribution pattern between two pairs of microtubules (ΔL_{DP} in Fig. 5) is one-fourth of the total length of the elastic flagellar model.

(7) The sliding velocity between adjacent microtubules is constant and independent of the location

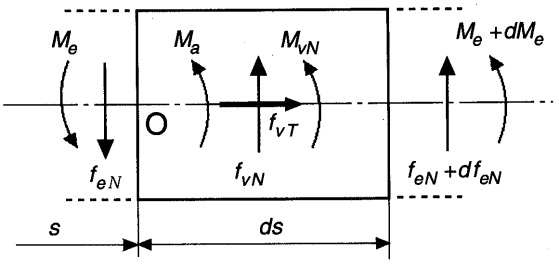

Fig. 6 Balance of force and moment on microlength segment

and the extent of the sliding region.

(8) The extent of the sliding region e_s changes as

$$\begin{cases} e_s = s_{sl} & (0 < s_{sl} < e_{s\max}) \\ e_s = e_{s\max} & (e_{s\max} < s_{sl} < S_{TL} - e_{s\max}) \\ e_s = e_{s\max} - s_{sl} - (S_{TL} - e_{s\max}) & (e_{s\max} < s_{sl} < S_{TL} - e_{s\max}) \end{cases}, \quad (4)$$

where s_{sl} is the distance between the origin of the coordinate axes and the end of the sliding region along the longitudinal axis and $e_{s\max}$ is the maximum value of e_s. s_{sl} is written by

$$s_{sl} = vt . \quad (5)$$

(9) The sliding length in the sliding region l_s is proportional to the extent of the sliding region and given by

$$l_s = \frac{l_{s\max}}{e_{s\max}} e_s . \quad (6)$$

(10) Active sliding at the top of the flagellar model is restricted.

(11) No twisting of the flagellar model occurs around its longitudinal axis during bending.

5. Basic Equations

5.1 Bending form[1),(2)]

5.1.1 Balance of force and moment Figure 6 shows the balance of force and moment on the microlength segment ds of the elastic flagellar model. The force balance on the microlength segment of the elastic flagellar model can be formulated as

$$f_{eN} = (f_{eN} + df_{eN}) + f_{vN} , \quad (7)$$

where f_{eN} is the normal component of the force acting on ds, and f_{vN} is the normal component of the viscous drag resistance.

The moment balance on O of the microlength segment of the elastic flagellar model can be formulated as

$$M_e + M_v + M_a + (M_e + dM_e) + (f_{eN} + df_{eN})ds = 0 , \quad (8)$$

where M_a, M_e and M_v are, respectively, the active bending moment exerted by sliding of microtubules, the moment produced by an elastic back force under the influence of viscosity, and the moment produced by a viscous drag resistance. M_a is given by

$$M_a = \frac{EI}{r_c} , \quad (9)$$

where E is Young's modulus, and I is the geometrical moment of inertia of the elastic flagellar model. M_v is given by

$$M_v = \frac{f_{vN} ds}{2} . \quad (10)$$

M_e is calculated from Eq. (8).

5.1.2 Viscous force Since the Reynolds number of the elastic flagellar model is exceedingly small, basic equations of the force acting on the flagellar model while it is moving in liquid are applied to the resistive force theory[5]. The tangential and normal components of viscous drag forces on the microlength segment ds of the elastic flagellar model are

$$\begin{aligned} f_{vT} &= -C_T\{v_x \cos\phi + v_y \sin\phi\} ds \\ f_{vN} &= C_N\{-v_x \sin\phi + v_y \cos\phi\} ds \end{aligned} , \quad (11)$$

where C_N and C_T are, respectively, tangential and normal viscous drag coefficients[2]. ϕ is the angle at which the tangential line of ds intersects the x axis. v_x and v_y are, respectively, the x and y directional moving velocities of the microlength segment.

$$C_N = \frac{-2\pi\mu}{\ln\frac{D}{2\lambda} + 0.5} \quad (12)$$

$$C_N = 2C_T \quad (13)$$

where λ is the wavelength.

5.1.3 Shape of the elastic flagellar model The shape of the elastic flagellar model is expressed in terms of the angle at which the tangential line of ds intersects the x axis, ϕ. $d\phi$ is given from the moment produced by an elastic back force under the influence of viscosity M_e:

$$d\phi = -\frac{M_e}{EI} ds . \quad (14)$$

ϕ at the arbitrary point on the elastic flagellar model is given by the integral along the longitudinal axis:

$$\phi = -\int_0^s \frac{M_e}{EI} ds . \quad (15)$$

5.2 Thrust force

The thrust force on the microlength segment of the elastic flagellar model is

$$f_x = f_{vN} \sin\phi - f_{vT} \cos\phi . \quad (16)$$

To evaluate the maximum x-directional thrust force, we assumed that the swimming speed of the flagellar model is zero. The x-directional thrust force of the flagellar model is given by

$$F_x = \int_0^{S_{TL}} f_x ds . \quad (17)$$

6. Simulation Method

The simulation was carried out according to the flowchart shown in Fig. 7. A small fraction of time Δt was set at 1/400 of a bending cycle. Specifications of

Table 1 Specifications of the elastic flagellar model

Total Length: S_{th}	30 μm
Diameter of flagellar model: D	0.2 μm
Distance between adjacent microtubules: a	0.14 μm
Frequency: f	35 Hz
Maximum value of the extent of sliding region: e_{smax}	3.0 μm
Maximum value of the sliding length: ℓ_{smax}	0.071～0.283 μm
Young's modulus of the elastic flagellar model: E	0.01～10.00 GPa
Coefficient of viscosity of liquid: μ	1.002～100.2×10^{-4} Ns/m^2

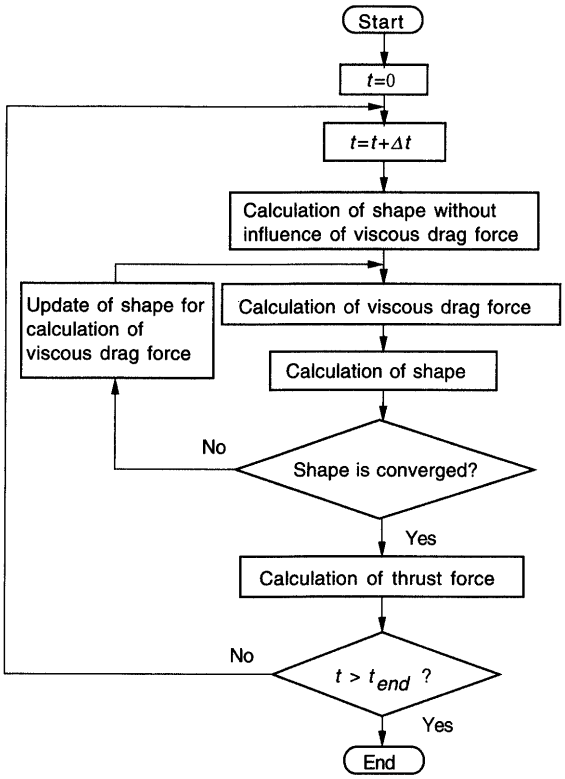

Fig. 7 Flowchart of simulation

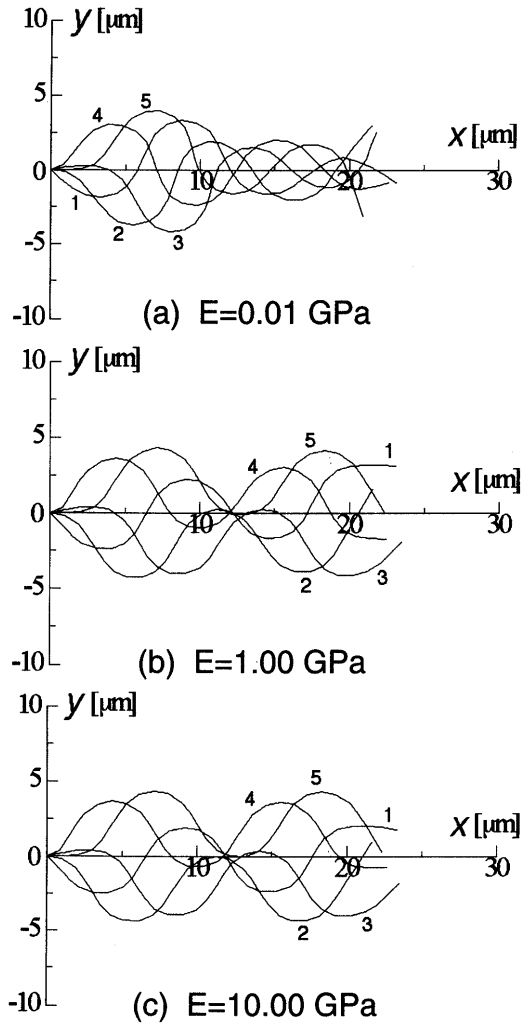

Fig. 8 Movement pattern of elastic flagellar model during one cycle. Maximum sliding length $l_{s\,max}$= 0.141 μm, coefficient of viscosity of liquid μ=1.002×10^{-4} Ns/m^2

the elastic flagellar model are given in Table 1. The frequency is based on sea urchin spermatozoa[7]. Young's moduli of the actual microtubules (2-9 GPa[8],[9]) are within the range of E. The standard value of the coefficient of viscosity μ is 1.002×10^{-4} Ns/m^2 (water at 25°C). As the maximum value of the sliding length $l_{s\,max}$, we defined $l_{s\,max}$=0.141 μm, which causes 1.0 rad of bending angle θ when the sliding region is set at 1/4 of the total length from the top in the absence of viscosity, as the standard value. The number of microlength segments in the elastic flagellar model was set at 300.

We used a computer (VR460-HP9000/800, Hitachi, Ltd.) for the simulation.

7. Results and Discussion

7.1 Elasticity of the elastic flagellar model

Figure 8 demonstrates the movement patterns of three elastic flagellar models with different elasticities during one bending cycle. Although the top of the elastic flagellar model is fixed in conformity with the basic conditions for modeling, the bending form is similar to the movement of flagella. For the lowest value of Young's modulus (E=0.01 GPa) shown in Fig. 8(a), the amplitude of bending on the posterior half is reduced. This is explained by the fact that the deformation by viscous drag resistance increases with increasing distance from the top of the elastic flagellar model, because the top of the model is fixed as mentioned as the basic conditions for modeling. In the case of free swimming (top of the model is not fixed), the reduction of the amplitude of the posterior half would be lessened. For higher values of Young's modulus (E=1.00 and 10.00 GPa) shown in Figs. 8(b) and (c), the bending movement of these flagellar models shows a "throat" in the middle of the longitudinal

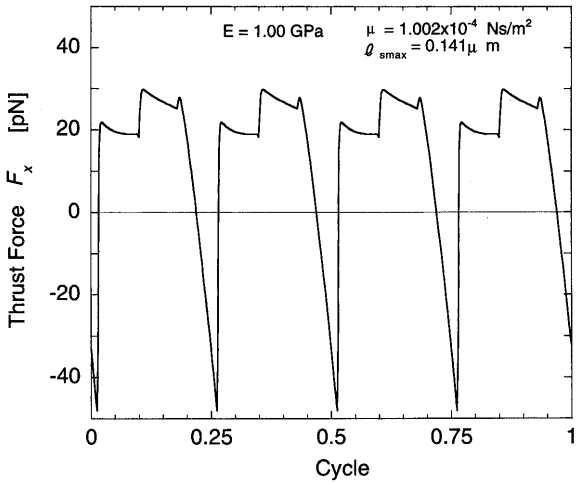

Fig. 9 Variation of thrust force F_x of elastic flagellar model during one cycle

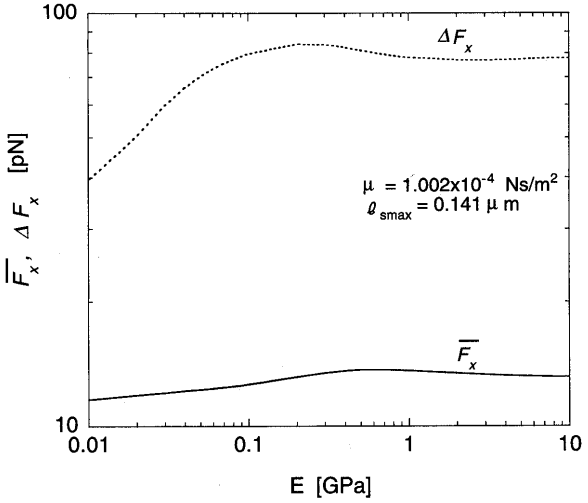

Fig. 10 Thrust force versus Young's modulus E

axis and almost the same amplitudes of bending for the anterior half and the posterior half.

Figure 9 shows the variation of thrust force F_x of the elastic flagellar model during one bending cycle. This figure indicates four cycles of thrust force in one bending cycle, and four steep changes of the thrust force. It is suggested that the sudden changes of the moving vector at the beginning of active sliding are responsible for the steep changes of the thrust force. This characteristic of the variation in the thrust force does not change with Young's modulus, the maximum sliding length and the viscosity of liquid. Figure 10 shows the thrust force versus Young's modulus E. The thrust force average $\overline{F_x}$ does not change greatly but decreases with a decrease in E lower than around 0.7 GPa. Besides, the thrust force difference ΔF_x ($= F_{x\max} - F_{x\min}$) is reduced markedly with a decrease in E lower than around 0.1 GPa. This can be accounted for by the bending movement of the model: Bending

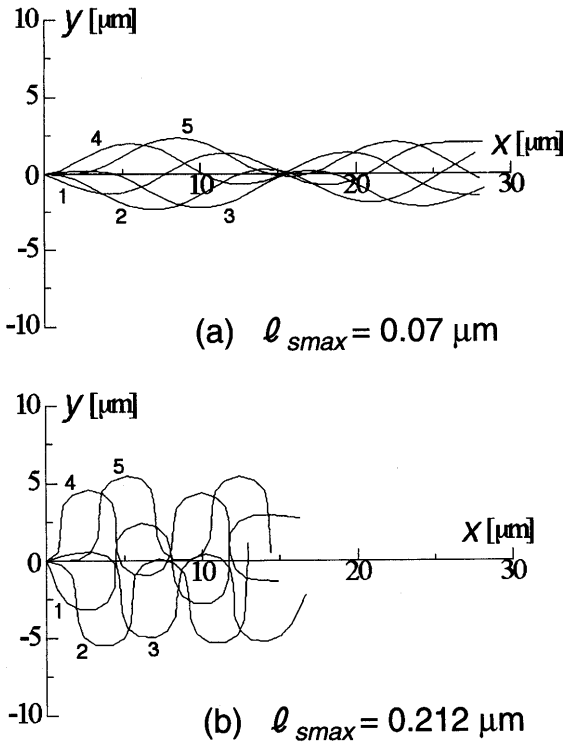

Fig. 11 Movement pattern of elastic flagellar model during one cycle. Young's modulus E=1.00 GPa, coefficient of viscosity of liquid μ=1.002×10^{-4} Ns/m^2

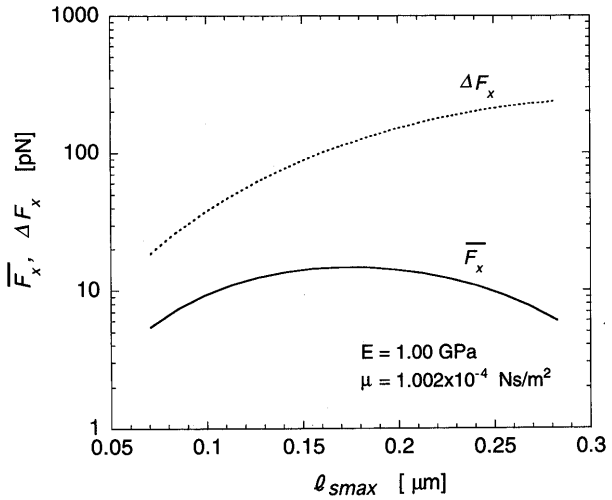

Fig. 12 Thrust force versus maximum sliding length $l_{s\max}$

movement does not change greatly at E values greater than 1.00 GPa; however, bending movement changes to reduce the amplitude in the posterior half at E values less than 1.00 GPa.

7.2 Sliding length

Figure 11 demonstrates the movement patterns of two elastic flagellar models with different maximum sliding lengths $l_{s\max}$ during one bending cycle. The sinuousness (corresponding to the ratio of amplitude to wavelength, A/λ) of the model increases with increasing $l_{s\max}$. Figure 12 shows the thrust force

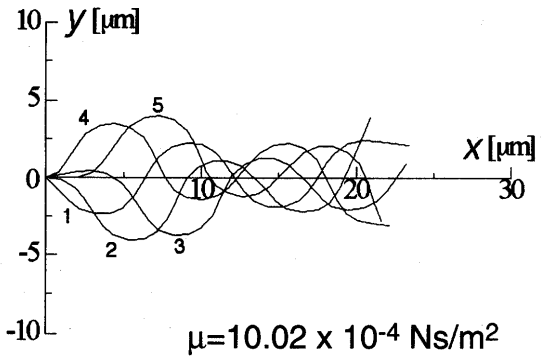

Fig. 13 Movement pattern of elastic flagellar model during one cycle. Young's modulus E=1.00 GPa, maximum sliding length $l_{s\,max}$= 0.141 μm, coefficient of viscosity of liquid $\mu=10.02\times10^{-4}$ Ns/m^2

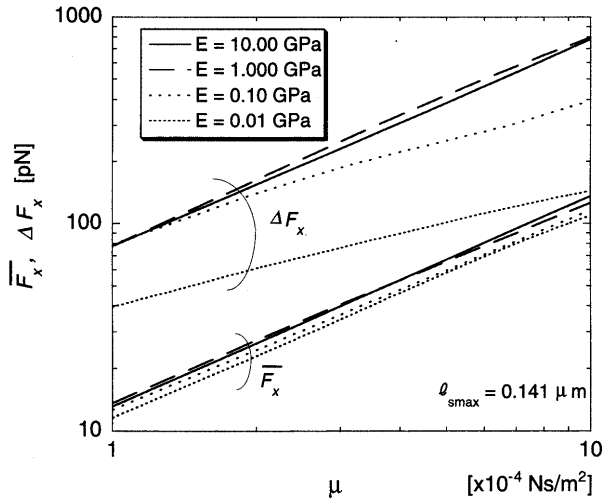

Fig. 14 Thrust force versus coefficient of viscosity of liquid μ

versus the maximum sliding length $l_{s\,max}$. The thrust force difference ΔF_x increases with an increase in $l_{s\,max}$. However, the thrust force average becomes a maximum around $l_{s\,max}$=0.017 μm and decreases with a further increase in $l_{s\,max}$. These indicate that the excessive sinuousness of the elastic flagellar model is not effective for its propulsion.

7.3 Viscosity of liquid

Figure 13 demonstrates the movement pattern of the elastic flagellar models in viscous liquid (the coefficient of viscosity $\mu=10.02\times10^{-4}$ Ns/m^2, 10 times the viscosity of water at 25°C). The amplitude of bending on the posterior half is reduced by the viscous drag resistance. This movement is the same as the movement at E of 0.1 GPa and μ of 1.002×10^{-4} Ns/m^2. This indicates that the elasticity of the elastic flagellar model and the viscosity of liquid are the relative for the bending movement. Figure 14 shows the thrust force versus the coefficient of viscosity of liquid μ. The thrust force increases with an increase in viscosity. There are no great differences in $\bar{F}_x$ and ΔF_x between the models of E=1.00 and 10.00 GPa. Furthermore, this figure indicates two points: (1) a higher elasticity is desirable for generating a higher thrust force average, (2) a lower elasticity is desirable for generating a lower thrust force difference.

8. Conclusions

This study was conducted to simulate the bending movement and the thrust force of the elastic flagellar model, and to determine the influences of elasticity, maximum sliding length and viscosity of liquid on the bending movement and the thrust force. The following results were obtained.

(1) For a low value of Young's modulus (E=0.01 GPa), the amplitude of bending on the posterior half is reduced by the viscous drag resistance.

(2) The elastic flagellar model shows four cycles of the thrust force in one bending cycle.

(3) The sinuousness of the model increases with the increase in the maximum sliding length. The excessive sinuousness of the elastic flagellar model is not effective for its propulsion.

(4) For propulsion in a highly viscous liquid, a higher elasticity is desirable for generating a higher thrust force average, and a lower elasticity is desirable for generating a lower thrust force difference.

Problems to be solved in the future include: (1) calculation of sliding force in the sliding region, and (2) definition and evaluation of the efficiency for propulsion.

Acknowledgements

The authors are deeply grateful to Dr. S. Kamimura of the University of Tokyo for his continuing guidance.

This work was supported by a research grant of the Research Foundation for the Electrotechnology of Chubu, a financial assistance of FANUC FA and Robot Foundation and a Grant-in-Aid for COE Research (10CE2003) by the Ministry of Education, Science, Sports and Culture of Japan.

References

(1) Sugino, K. and Naitoh, Y., Simulated Cross-Bridge Patterns Corresponding to Ciliary Beating in Paramecium, Nature, Vol. 295 (1982), pp. 609-611.

(2) Sugino, K. and Naitoh, Y., Computer Simulation of Ciliary Beating in Paramecium, J. Sunmicrosc. Cytol., Vol. 15, No. 1 (1983), pp. 37-42.

(3) Kobayashi, S., Shibasaki, Y. and Morikawa, H., Simulation Study for Micropropulsion Mechanism in Liquid Modeled on Sliding Mechanism of

Microtubules in Flagella, JSME Int. J., Ser. C, Vol. 42, No. 3 (1999), pp. 730-736.
(4) Kobayashi, S., Fukuda, K. and Morikawa, H., Simulation Study for Three-Dimensional Micro-propulsion Mechanism Modeled on Bending Mechanism of Eukaryotic Flagella in Liquid, JSME Int. J., Ser. C, Vol. 42, No. 3 (1999), pp. 777-783.
(5) Okajima, A. and Maruyama, K., Undo To Kodo, (in Japanese), (1975), p. 180, Iwanami Shoten.
(6) Murase, M., The Dynamics of Cellular Motility, (1992), pp. 102-111, John Wiley & Sons.
(7) Gray, J. and Hancock, G.J., The Propulsion of Sea-Urchin Spermatozoa, J. Exp. Biol., Vol. 32 (1955), pp. 802-814.
(8) Tolomeo, J.A. and Holley, M-C, Mechanics of Microtubule Bundles in Pillar Cells from the Inner Ear, Biophysical Journal, Vol. 73, No. 4 (1997), pp. 2241-2247.
(9) Gittes, F., Mickey, B., Nettleton, J. and Howard, J., Flexural Rigidity of Microtubules and Actin Filaments Measured from Thermal Fluctuations in Shape, J. Cell Biology, Vol. 120, No. 4 (1993), pp. 923-934.